

Published in final edited form as:

Cancer Res. 2019 April 15; 79(8): 1884–1898. doi:10.1158/0008-5472.CAN-18-2553.

MDH1 and MPP7 regulate autophagy in pancreatic ductal adenocarcinoma

Maria New^{#1}, Tim Van Acker^{#1}, Jun-ichi Sakamaki², Ming Jiang³, Rebecca E. Saunders³, Jaclyn Long², Victoria M.-Y. Wang⁴, Axel Behrens⁴, Joana Cerveira⁵, Padhmanand Sudhakar^{6,7}, Tamas Korcsmaros^{6,7}, Harold B. J. Jefferies¹, Kevin M. Ryan², Michael Howell³, and Sharon A. Tooze^{¶,1}

¹Molecular Cell Biology of Autophagy Laboratory, The Francis Crick Institute, London, UK

²Tumour Cell Death Laboratory, Cancer Research UK Beatson Institute, Glasgow, UK

³High Throughput Screening, The Francis Crick Institute, London, UK

⁴Adult Stem Cell Laboratory, The Francis Crick Institute, London, UK

⁵Flow cytometry, The Francis Crick Institute, London, UK

⁶Korcsmaros Group, Earlham Institute, Norwich, UK

⁷Korcsmaros Group, Quadram Institute, Norwich, UK

These authors contributed equally to this work.

Abstract

Pancreatic ductal adenocarcinoma (PDAC) is driven by metabolic changes in pancreatic cells caused by oncogenic mutations and dysregulation of p53. PDAC cell lines and PDAC-derived xenografts grow as a result of altered metabolic pathways, changes in stroma, and autophagy. Selective targeting and inhibition of one of these may open avenues for the development of new therapeutic strategies. In this study, we performed a genome-wide siRNA screen in a PDAC cell line using endogenous autophagy as a readout and identified several regulators of autophagy that were required for autophagy-dependent PDAC cell survival. Validation of two promising candidates, MPP7 (MAGUK p55 subfamily member 7, a scaffolding protein involved in cell-cell contacts) and MDH1 (cytosolic Malate dehydrogenase 1), revealed their role in early stages of autophagy during autophagosome formation. MPP7 was involved in activation of YAP1 (a transcriptional coactivator in the Hippo pathway), which in turn promoted autophagy, whereas MDH1 was required for maintenance of the levels of the essential autophagy initiator serine-threonine kinase ULK1, and increased in activity upon induction of autophagy. Our results provide a possible explanation for how autophagy is regulated by MPP7 and MDH1, which adds to our understanding of autophagy regulation in PDAC.

¶Corresponding author: Sharon A. Tooze, The Francis Crick Institute, 1 Midland Road, London NW1 1AT UK, (+44) (0) 203 796 1340, Sharon.tooze@crick.ac.uk.

Conflict of interest

The authors declare no potential conflicts of interest

Keywords

PDAC; ULK1; WIPI2; LC3; autophagosome; proteasome; hypoxia

Introduction

Pancreatic ductal adenocarcinoma (PDAC) is a cancer of unmet need with a median patient survival of only 6-9 months (1). Key PDAC features include a high rate of activating KRAS mutations, a hypervascular and hypoxic microenvironment and reprogramming of cellular metabolism (2).

A number of studies have linked autophagy to PDAC survival and progression. Autophagy is constitutively activated in PDAC cell lines and tumours (3). This is required for tumour cell survival, as demonstrated by either pharmacological or genetic autophagy inhibition resulting in loss of viability in cell models and PDAC xenografts (4). Despite current advances, PDACs become resistant to most therapies, and new treatment avenues are urgently needed.

Macroautophagy (hereafter autophagy) is an essential, evolutionarily conserved membrane-mediated process that delivers cytoplasmic constituents in double-membraned autophagosome vesicles to lysosomes for degradation, energy release, and component recycling (5). Mammalian autophagy is mediated by at least 18 autophagy (ATG) proteins acting in a concerted hierarchy (6). The mammalian ATG8s, which include LC3B, are used to monitor autophagosome formation and autophagic flux (7). Autophagy has a homeostatic role under basal conditions, eliminating damaged organelles and misfolded proteins that may otherwise diminish cellular fitness and integrity. Autophagy is also induced in response to stimuli including starvation, hypoxia, and other stresses to ensure cell survival.

The role of autophagy in cancer is complex and context-dependent with evidence for both tumour-survival and tumour-suppressive roles. Autophagy is thought to be required for anti-cancer immunosurveillance and inhibition of malignant transformation. However, in established tumours, autophagy can also provide a means for tumour cell survival and therapy resistance (8). In PDAC, autophagy is constitutively activated (9) and required for tumour development, metabolism and growth (4, 10).

Although the importance of autophagy in cancer is established, the process is still not fully understood, and it remains unclear how manipulation of autophagy in PDAC should be optimally deployed for clinical benefit. There is therefore a need for discovery of novel autophagy regulators, as the enhanced understanding of autophagy may yield new therapeutic targets.

To identify of novel targets we performed a genome wide loss-of-function screen to identify genes that regulate autophagy in PDAC cells. Regulators identified through the screen will elucidate molecular mechanisms governing tumour cell survival and autophagy. We report that levels of MPP7 and MDH1 influence autophagic flux under basal and hypoxic conditions. Our ATG protein-pathway mapping experiments show MPP7 and MDH1

influence the earliest stages of autophagy. Furthermore, our results suggest that YAP1 may contribute to the positive regulation of autophagy by MPP7, and reveal a functionally important role for MDH1 in maintaining cellular ULK1 levels. Exploiting the apparent sensitivity of PDAC to autophagy inhibition provides a rational basis for the consideration of these novel autophagy regulators as therapeutic targets.

Materials and methods

Cell culture and reagents

Cell lines were ordered from ATCC (BxPc-3, Panc 02.03, Panc 10.05, Panc-1, PL45), Riken (KLM-1, KP4-3, PK-1, PK-45H), JCRB (SUIT-2, KP-4, KP-2) and DSMZ (HUPT3, YAPC, PA-TU-8902, PA-TU-8999, DAN-G), expanded, fluorescence based mycoplasma testing was performed, followed by agar culture confirmation. A large batch of cells was frozen. Cells were passaged twice a week and used until 20 passages. All PDAC cell lines were grown in full medium: DMEM with 10% fetal calf serum and 4 mM L-glutamine.

PK-1 cell lines stably expressing Tet-On inducible myc-tagged MDH1 and Tet-On inducible HA-tagged MPP7 were maintained in DMEM with 10% tetracycline-free fetal calf serum, 4 mM L-glutamine and 1 µg/ml puromycin.

Where indicated, cells were treated with 100 nM Bafilomycin A1 (Calbiochem), 100nM Torin1 (Cayman Chemical), 100 nM epoxomicin (Sigma) or for 24 hours with 1 µg/mL doxycycline (Takara Bio). For autophagy induction by amino-acid starvation, cells were washed 3 times in Earle's balanced salt solution (EBSS) and incubated in EBSS for 4 hours.

Lipofectamine 3000 (ThermoFisher) was used for transient transfection of PK-1 cells according to manufacturer's instructions. DNA plasmids were used at a concentration of 1.5 µg/ml of transfection mix.

siRNA transfection was carried out for 72 hours with a final concentration of 50 nM siRNA, using Lipofectamine RNAiMAX (ThermoFisher) according to manufacturer's instruction. All siRNA oligos used were purchased from Dharmacon. For knockdown and rescue experiments, reverse siRNA transfection was performed on day 1, and transfection with DNA 48 hours later, 24 hours prior to cell harvesting. Immunoblotting was carried out as previously described (11).

Confocal and epifluorescence microscopy were carried out as previously described (12) and LC3 puncta formation was quantified by Imaris image analysis software.

siRNA screens

The siGENOME SMARTpool human siRNA genome library and deconvoluted siGENOME SMARTpools (Dharmacon) were used in triplicate at a final siRNA concentration of 18.75 nM with 0.0075 µl/well of INTERFERin-HTS reagent (Polyplus), and 600 cells/well in a final volume of 50 µl/well in black and clear bottom 384-well plates (Greiner). siRNA libraries were aliquoted on a Beckman FX liquid handling station and all other liquid addition steps performed with a FluidX Xrd-384 plate dispenser. Following reverse siRNA

transfection, plates were incubated at 37 C in 5% CO₂ for 72 hours, with Bafilomycin A1 at a final concentration of 50 nM present for the final 6 hours of transfection. Cells were then fixed in 4% paraformaldehyde (Sigma) for 30 minutes, followed by incubation with methanol for 15 mins and staining with primary (anti-LC3 5F10 antibody (nanoTools Antikörpertechnik) (used at 1:100 dilution in 1% BSA) and secondary antibody (anti-mouse Alexa Fluor 488 Life Technologies at 1:1000 dilution in 1% BSA).

Image capture and data analysis

To collect antibody labelling and nuclear a Thermo Scientific Cellomics Arrayscan Vti (20x magnification, 0.4 NA, BGRFR filter set, X1 camera, LED illumination) and accompanying image analysis software were used (8 fields scanned per well). The parameters recorded were: number of nuclei (object count) from the DAPI channel; number of LC3 spots/cell; total spot count; total spot area; average spot area; total spot intensity and average spot intensity. More detailed descriptions of algorithm parameters are available upon request.

Raw data for the individual parameters was normalised to correct for plate, row and column effects, then divided by the individual plate median absolute deviation, thus creating a Z-score. Replicates were summarised by taking the median Z-score for each siRNA pool and normalised scores for the three parameters were then combined into a ranked list, thereby determining the top 200 spot decreaseers for the primary siGENOME screen. For the secondary deconvolution screen, results are expressed as percentage of control (POC) with respect to the RISCfree control (median of 3 replicates).

Bioinformatic analysis

For the promising targets generated from the genome-wide siRNA screen experiments, molecular interaction information comprising protein-protein interactions (PPIs) and transcriptional regulatory interactions (TRIs) were retrieved from the Autophagy Regulatory Network (ARN) (13). PPIs and TRIs were also retrieved from IntAct (14), HPRD (15) and HTRI (16), ORegAnno (17) databases respectively. In addition, the annotation (core autophagy protein, post-translational regulator, transcriptional regulator etc) of the target proteins was also derived from ARN. In order to select the targets which could have the highest effects on autophagy, they were ranked based on the cell viability z-score (≥ -1.5 and ≤ 1.5), expression status in pancreatic cancer (source : Human Protein Atlas - (18)), presence of core autophagy interactors and visual imaging. From the above-mentioned analysis, the top 25% of the hits identified as being relevant modulators of autophagy in pancreatic cancer were selected. Based on the effects on long term cell viability, targets with lethal effects were discarded. To further shortlist the targets, we developed an aggregated score for each target to determine its cumulative effect on autophagy. The aggregated score was based on read-outs from experimental screens (measuring the differential effects on viability of autophagy dependent and autophagy independent PDAC cells) in addition to possible modes of action inferred from interaction networks. We used PPIs and TRIs to determine if there are any direct or indirect connections from the shortlisted targets to any of the 37 core autophagy proteins. The aggregated score was then calculated for each shortlisted target based on the expression (source : Human Protein Atlas - (18)) and methylation levels (source PCMDB - (19)) in pancreatic cancer, acumen cell number and cell

viability scores of the intermediary proteins connecting the targets with the core autophagy proteins. The average aggregated score for each target was then calculated by dividing the aggregated score by the total number of intermediary proteins through which the target could potentially mediate its effects on the core autophagy proteins. Targets with no direct or indirect interactions (via intermediary proteins) with core autophagy proteins were discarded from further analysis.

High throughput growth assay

Single siRNA oligos (50 nM final concentration) were reverse transfected in PK-1, PA-TU-8902, KP-4 and SUI2-2 cells in 96-well format using 0.03 μ l Lipofectamine RNAiMAX/well. Three cell numbers were plated for each cell line. For PK-1 cells, 750, 1000 and 2000 cells were seeded/well, for PA-TU-8902 500, 1000 and 2000 cells/well, for KP-4 250, 500 and 1000 cells/well and for SUI2-2 125, 250 and 500 cells/well. Each hit-targeting siRNA was tested in quadruplicate wells for each cell number. Control siRNA were tested in duplicate wells. Seven days after transfection, cells were fixed using 4% PFA and cell proliferation was assessed by Hoechst staining and scanning on TTP Labtech's acumen Cellista.

qPCR

72 hours post-transfection, qPCR samples were harvested and RNA was extracted using the RNeasy Mini Kit (Qiagen) followed by cDNA production using SuperScript II Reverse Transcriptase (Life Technologies). qPCRs were performed with Fast SYBR Green Master Mix (Thermo Scientific) and relative mRNA expression levels were calculated.

MDH1 activity assay

Cells were lysed in NP-40 buffer supplemented with a protease inhibitor (Roche), and immunoprecipitated with anti-myc agarose beads (Chromotek) for 2 hours. The immunoprecipitated beads were washed 3 times with NP-40 buffer, and the on-beads activity of myc-MDH1 was determined by measuring the decrease in the fluorescence of NADH (Ex. 350 nm; Em. 470 nm) on an EnVision 2102 multilabel plate reader. The reaction was monitored at 15-second intervals for 20 minutes. This protocol was adapted from {Kim, 2012 #23072}.

Annexin V assay

PK-1 and KP-4 cells were harvested into single cell suspension, washed once in PBS and resuspended in 1x Annexin V binding buffer (10x commercial buffer diluted in distilled water, BD Pharmingen, Cat 51-6710AK). To each 500 μ l of cell suspension 2.5 μ l of FITC-conjugated annexin V antibody were added and incubated for 15 minutes at room temperature. To identify dead cells, 4',6-Diamidino-2'-phenylindole dihydrochloride (DAPI, Sigma, Cat D8417) was added to the samples to a final concentration of 2 μ M just before running them on the flow cytometer.

Annexin V signal was detected using a CS&T-calibrated BD LSRFortessa system (Becton Dickinson, Carlsbad, USA) configured with a 355nm, 405nm, 488nm, 561nm and 633nm laser excitation lines and associated detector arrays. Annexin V-FITC was detected in the

530/30 blue detector and DAPI was detected in the 450/50 UV detector. Acquisition gates were set using FACS DIVA software (v 8.0.1, Becton Dickinson, Carlsbad, USA) and a minimum of 30,000 single events were collected. Post-acquisition analysis was performed using FlowJo software (version 10.1, Tree Star, Inc.). Briefly, intact cells were selected on FSC-A v SSC-A plot. Single cells were then selected using the area and the height from SSC. Live, apoptotic and necrotic/dead cells were identified using a spider quadrant gate.

Organoid formation assay

Primary murine PDAC cells were isolated from Pdx1-Cre, KRas^{G12D}, p53 fl/fl mouse pancreases (20) when tumours were palpable, and grown as three-dimensional organoids in Matrigel as previously described (21). All experiments performed in animals were approved by the Francis Crick Institute's Animal Welfare and Ethical Review Body, and conformed to UK Home Office regulations under the Animals (Scientific Procedures) Act 1986 including Amendment Regulations 2012." Cells were cultured in advanced Dulbecco's Modified Eagle Medium/F12 medium with 10 % FCS, Pen/Strep (1x), 10 % Noggin-condition media, 10 % R-spondin-condition media, B27 Supplement (1x), Nicotinamide (10 mM), N-acetyl cysteine (1.25 mM), EGF (0.05 µg/ml), FGF (0.05 µg/ml) and Gastrin (0.01 µM). pGIPZ shRNAs targeting MPP7 and Atg5 (Dharmacon) were subcloned into the doxycycline-inducible pTRIPZ vector. Stable KPC organoids expressing each construct were then created using lentiviral transduction, passaged three times, and equal cell numbers for each construct were sorted on a BD FACSAria Fusion (BD Biosciences) into 96-well plate wells containing Matrigel. Organoid growth was assessed 6 days after the FACS sort, and organoid number quantified with ImageJ.

Results

Genome-wide screen identifies novel regulators of autophagy in PDAC cell lines

To identify novel regulators of autophagy in PDAC, a multistep screening and validation approach was undertaken, see workflow in Figure 1A. The aim of the screen was to identify proteins essential for autophagy, measured by LC3 puncta levels upon Bafilomycin A1 (BafA1) treatment, which is an inhibitor of the vacuolar-type H⁺-ATPase found in endosomes and lysosomes (7). BafA1 was used as a tool to measure accumulated LC3 as it prevents its degradation in autophagosomes. LC3 puncta form upon activation of autophagy by the canonical pathway initiated by ULK1 activation and production of phosphatidylinositol-3-phosphate (PI3P) (5), and recruitment of WIPI2 (12), leading to lipidation of LC3 (thus forming LC3-II) on autophagosomes. Under steady-state conditions, basal autophagy proceeds using the same machinery but typically at a reduced level.

A selection was made of suitable cell lines for high-throughput genome-wide screening, and subsequent validation and hit selection. We aimed to identify an appropriately adherent cell line with high autophagic flux. Seventeen PDAC cell lines were assayed in normal growth medium with and without BafA1. LC3 puncta were detected by antibody labelling, and LC3-II was detected by western blot. Autophagic flux was determined by the fold induction of LC3 puncta and LC3-II upon BafA1 treatment (Figure 1B and C). Based on its high

autophagy flux and suitability for imaging in the high-throughput format, the KP-4 cell line was selected for the siGENOME screen.

The siGENOME screen was performed in triplicate under 6 hours of BafA1 treatment, using a whole genome SMARTpool siRNA library. After fixation, multiple images of each well were taken, and endogenous LC3 puncta and nuclei were identified (Figure 1D). Effects of each siRNA SMARTpool on LC3 puncta number were assessed by measuring related parameters, such as number, intensity, and area. Knockdown of known essential autophagy regulators such as ATG4B and BECN1 decreased the measured parameters as expected, e.g. spot total area per object (STAPO) Z-score (Figure 1E). Normalized Z-scores for the various LC3 (Ch2) parameters were combined for each gene to give a weighted binary score and allow us to create a ranking of autophagy regulators. Numerical values of normalized Z-scores for these parameters for each siRNA SMARTpool of the top 200 positive autophagy regulators are presented in Supplementary Table 1.

Next in the deconvolution screen, the top 200 puncta-decreasing targets from the genome-wide primary screen were screened again with four siRNAs for each target to confirm the primary screen results (Supplementary Table 2). The results of the deconvolution screen were subsequently integrated with the results of the primary screen. In order to identify robust autophagy modulators, we used systems and network biology concepts to rank the shortlisted hits. While the LC3 puncta-related parameters were derived from the primary screens, we carried out a molecular interaction network-based bioinformatic analysis to identify how the selected targets could affect autophagy either directly via interactions with core autophagy proteins or indirectly via other intermediary proteins. As a source of molecular interactions specific to autophagy, we used the Autophagy Regulatory Network (ARN) resource (13). In addition, expression of the analysed targets in pancreatic cancer was retrieved from the Human Protein Atlas database (18) and used to incorporate context specificity in the ranking process. Inferences from the visual interrogation of the primary image data were also incorporated to increase confidence in the primary screen hits. We selected the top 25% of the hits from the above analysis to further proceed with the shortlisting and experimental verification. Hence, using multiple indicators such as LC3 puncta-related parameters, molecular network related properties, context specificity and visual imaging, we created a shortlist of relevant and probable autophagy modulators in the context of pancreatic cancer and their possible interactions.

Identification of autophagy regulators that affect autophagy-dependent PDAC cell proliferation

A number of previous studies suggested a role for autophagy in pancreatic cancer cell survival (4, 10). We determined whether the survival of the 17 PDAC cell lines we studied was dependent upon autophagy. To achieve this, CRISPR knockout of the essential autophagy genes Atg5 and Atg7 was performed, followed by cell proliferation measurements. While multiple cell lines show dependence on autophagy, PK-1, PA-TU-8902, and KLM-1 show the greatest dependency on autophagy for survival while the remaining cell lines tested, KP-4, SUI-2 and others (Figure 1F-M, Supplementary Figure 1A-L) are much less dependent on autophagy for survival.

A 7 day proliferation assay was then carried out in the autophagy-dependent PK-1 cell line to establish how siRNA knock-down of the top 25% autophagy regulators we identified would affect cell survival (Figure 2A). Note, two siRNAs were selected from the deconvolution screen plus a number of controls. qPCR was carried out in parallel with the growth assay, and siRNAs which depleted target mRNA levels with 50% efficiency or higher were considered to have sufficient knockdown efficiency (Supplementary Table 3). Depletion of the majority of autophagy regulators caused some decrease in survival of autophagy dependent PK-1 cells compared to RISC-free siRNA (Figure 2A). Eleven targets were identified to have sufficient knockdown and cell survival reduced by 50% or more (Figure 2B).

Subsequently we determined which of the 11 targets regulate autophagy in the autophagy-dependent PK-1 cell line. Note, siRNAs for the 11 targets were chosen based on qPCR data and not all targets had 2 suitable siRNAs (GALNT1, GRIA3, MPP7, OPHN1 and UBR1 were only targeted by a single siRNA). After BafA1 treatment the effect of hit depletion on LC3 puncta number and intensity was quantified (Figure 2C and Supplementary Table 4). We next assayed if the targets were differentially required for survival in autophagy-dependent versus autophagy-independent cells using a long-term growth assay. Survival after siRNA depletion was tested in KP-4 and SUIT-2, two autophagy-independent, and PK-1 and PA-TU-8902, two autophagy-dependent cells lines (Figure 2D). Western blot analysis of LC3-II levels and qPCR to determine knock-down efficiency for 11 targets is summarized in Supplementary Figure 2.

Using the three criteria shown in Fig. 2B-D, MDH1 and MPP7 were identified as amongst the best regulators. Knock-down of MPP7 and MDH1 (02) reduced the proliferation of PK-1 cells (Fig. 2B), decreased LC3 puncta (Fig. 2C), and finally showed an enhanced loss of proliferation on the autophagy dependent cell lines (PK-1 and PA-TU-8902) compared to the autophagy-independent cell lines (KP-4 and SUIT-2). In addition, an important role for MDH1 in PDAC has been described (22–24), while MPP7 was relatively uncharacterized. Two other short-listed candidates (UBR1 and GALNT1) proved to be less robust in follow up assays.

MPP7 regulates basal and hypoxia-induced autophagy in PDAC

MPP7, MAGUK p55 subfamily member 7, has been shown to be required for epithelial tight junction formation (25), and for myoblast cell proliferation (26). A single siRNA duplex was used to knock down MPP7 in PK-1 cells, which inhibited LC3 lipidation both during amino acid starvation and BafA1 treatment (Figure 3A, 3B). Transient expression of an siRNA resistant mutant of MPP7 was able to rescue the levels of LC3-II after MPP7 knockdown (Figure 3C). These data confirm that MPP7 is a positive regulator of starvation-induced autophagy in PDAC cells. Using a stable, inducible PK-1 cell line expressing HA-tagged MPP7 we could modulate MPP7 levels. A significantly increase in LC3 puncta was seen upon MPP7 over-expression, compared to the doxycycline-treated controls (Figure 3D, 3E).

We determined whether MPP7 is required for hypoxia-induced autophagy as PDAC tumours exhibit a hypoxic microenvironment due to poor vasculature (27). High levels of hypoxia predict poor patient prognosis (28), hence a potential drug target may be especially useful.

Hypoxia is a known activator of autophagy (29), and in our experiments, both LC3-II levels and LC3 puncta increased in hypoxia-exposed cells (Figure 3F-I). MPP7 depletion results in a striking decrease of both LC3-II levels and LC3 puncta in hypoxia-exposed cells (Figure 3F- I), suggesting that MPP7 positively regulates not only basal, but also hypoxia-induced autophagy.

To identify the stage of autophagy MPP7 exerts its regulatory effect, ATG pathway mapping was performed under amino acid starvation. During initiation of starvation-induced autophagy, inactivation of mTORC1 and activation of ULK1 kinase occurs (30). ULK1 kinase activity is repressed by mTORC1 in nutrient-rich conditions, whereas starvation inhibits mTORC1 kinase activity, resulting in decreased ULK1 Ser757 phosphorylation and consequent ULK1 activation (31). To assess whether MPP7 is required for mTORC1 deactivation, phosphorylation of ULK1 Ser757 was measured during starvation. We found that MPP7 depletion appears to result in a slightly faster rate of ULK1 Ser757 dephosphorylation relative to controls (Figure 3J).

Downstream of mTORC1 and ULK1/2 in the autophagic pathway, WIPI2, a PI3P effector, is recruited to the forming autophagosome and mediates recruitment of the ATG12-ATG5-ATG16L1 complex, which is required for LC3 lipidation (12). WIPI2 then dissociates from formed autophagosomes. WIPI2 puncta formation is used to assess the recruitment of the class III PI3K lipid kinase complex I (7), a critical early requirement for autophagosome formation. MPP7 depletion significantly reduces WIPI2 puncta number under conditions of starvation (Figure 4A, 4B), providing further support that MPP7 may regulate autophagy at the initiation stage, and in particular PI3P levels.

MPP7 regulates autophagy through YAP1 activation

Based on bioinformatics analysis of MPP7 in the Autophagy Regulatory Network (13), we predicted that YAP1 (Yes-associated protein 1), a transcriptional regulator involved in cell proliferation and apoptosis suppression, may be involved in the regulation of autophagy by MPP7. Previous findings indicate that MPP7 is required for YAP1 accumulation in the nucleus, where it is transcriptionally active (26). Furthermore, YAP1 increases cellular autophagic flux in breast cancer cells, promoting breast cancer cell survival (32). We confirmed that YAP1 is required for both basal and starvation-induced autophagy in PK-1 cells (Figure 4C, 4D), as YAP1 depletion coincides with a reduction in LC3 lipidation both in fed and starved BafA1 treated cells. In addition, YAP1 depletion reduces hypoxia-activated autophagy (Figure 4E).

We observed depletion of MPP7 results in accumulation of YAP1, phosphorylated at S127 (Figure 4F) which is the cytoplasmic, inactive form of YAP1, confirming MPP7 is required for YAP1 activation (26). Overexpressed YAP1 in MPP7 depleted cells resulted in a rescue of autophagic flux (Figure 4G, 4H). Interestingly, the regulation of YAP1 activity and phosphorylation by MPP7 seems to be autophagy dependent, as ATG13 depletion appears to deactivate YAP1 (Figure 4I). Furthermore, in stable cell lines expressing WT and inactive S94A YAP1, inactive S94A YAP1 is unable to rescue autophagy (Figure 4J). In summary, our data demonstrate that MPP7 may positively regulates YAP1 activity in PDAC cells, and this may contribute to the positive regulation of autophagy by MPP7.

MDH1 regulates basal and hypoxia-induced autophagy in a PDAC cell line

MDH1 is known to be activated in human PDAC samples (23) and supports pancreatic cancer growth (22), and our findings indicate that MDH1 is required for both autophagy and survival in autophagy-dependent PDAC cells (Figure 2).

Like MPP7, MDH1 is required for both basal and starvation-induced autophagy: LC3 lipidation is reduced in starvation and BafA1 treatment when MDH1 is depleted (Figure 5A, B). Conversely, induction of myc-MDH1 using a stable doxycycline-inducible PK-1 cell line significantly increased the number of LC3 puncta, both with and without depletion of the endogenous protein (Figure 5C, D, E). MDH1 depletion significantly reduced hypoxia-induced autophagy, as demonstrated by a decrease in both LC3 lipidation and LC3 puncta (Figure 5F-I).

MDH1 regulates autophagy by maintaining ULK1 levels, and MDH1 is activated by autophagic stimuli

We next analysed the effect of MDH1 depletion on autophagy during amino acid starvation. Similar to MPP7, ULK1 pSer757 levels were reduced in amino acid starvation (Figure 6A). Pathway mapping analysis was carried out for MDH1 and similarly to MPP7, a reduction MDH1 coincided with reduced numbers of WIPI2 puncta under amino acid starvation, suggesting that MDH1 could also regulate autophagy in part through regulation of PI3K activity (Figure 6B and C).

However, we observed that ULK1 levels were reduced by depletion of MDH1 (Figure 6A, D and E). Conversely, induction of myc-MDH1 increased ULK1 levels (Figure 6F, 6G). Interestingly, under conditions of MDH1 depletion, inhibition of proteasome activity by epoxomicin treatment resulted in increased ULK1 levels, suggesting MDH1 may regulate ULK1 proteasomal degradation (Figure 6H). In support of this conclusion, epoxomicin treatment rescued autophagy under conditions of MDH1 depletion (Figure 6I, 6J).

We tested whether MDH1 regulation of ULK1 proteasomal degradation is specific to ULK1, or whether MDH1 also regulates proteasomal degradation of other proteins such as p53 and Mcl-1 (Figure 6K). We found that while proteasomal degradation of p53 does not appear to be regulated by MDH1, levels of Mcl-1, another protein involved in autophagy, decrease on MDH1 depletion, and rescued by proteasome inhibition. This suggests that the loss of MDH1 results in alterations of signalling upstream of the PI3K, and downstream of mTORC1, but MDH1 may regulate degradation of other proteins than ULK1.

Cytoplasmic MDH1 controls the production of malate by reduction of oxaloacetate, using the reducing power of NADH (33). MDH1 exists in two forms – the monomeric form, which is enzymatically inactive, and the active dimeric form (34). We found that autophagy induction through amino acid starvation and Torin treatment (to inactivate mTORC1) resulted in higher levels of the active form of MDH1. We found both higher levels of the dimerized form of MDH1 (Figure 7A, 7B and 7C), and an increased enzymatic activity of MDH1 as measured by assessing NADH conversion to NAD (Figure 7D and 7E). Hypoxic conditions also caused an increase in MDH1 dimer formation (Figure 7F and 7G). These

results suggest that MDH1 enzymatic activity is linked to its role in positively regulating autophagy.

MDH1 is monomethylated on Arg248, and this post-translational modification prevents dimerization and inhibits the catalytic activity of MDH1 (24). Mutation of the arginine (R248) to a phenylalanine (F) to mimic methylation (35), has previously been shown reduce the catalytic activity of MDH1 (24). Given the activation of MDH1 during autophagy induction, we determined whether the methylation of MDH1 affects its ability to regulate autophagy. Doxycycline-inducible myc-tagged MDH1 R248F cell lines were compared to inducible myc-MDH1 expressing cells. Whereas myc-MDH1 was able to rescue autophagy and ULK1 levels in siRNA depleted cells (Figure 7H, 7I), expression of the less catalytically active R248F mutant did not rescue autophagy levels (Figure 7J and 7K), suggesting that the catalytic activity of MDH1 is required for its role in autophagy.

Levels of MDH1, MPP7 and downstream autophagy regulators ULK1 and YAP1 affect PDAC cell survival

Using an organoid model of mouse PDAC (KRas^{G12D}, p53 fl/fl), and organoid formation as a readout for 'cancer stemness' and self-renewal (20), doxycycline-inducible knockdown of MPP7 and MDH1 reduced both organoid growth and autophagy levels (Figure 7L, M, and N). This provides further evidence for MPP7 and MDH1 being required for PDAC cell survival, not just of immortalized human PDAC cell lines, but also of primary organoids, a physiologically more relevant model system (21).

Furthermore, colony formation assays show that MPP7 and MDH1 depletion and depletion of their downstream autophagy regulators YAP1 and ULK1 reduces proliferation of the autophagy dependent PK-1 PDAC cell line. The reduction in viability of the autophagy independent KP-4 cell line is much less striking when these proteins are depleted (Supplementary Figure 3 A, B). To support this, Annexin V assays demonstrate that the population of necrotic and apoptotic cells increases when the autophagy regulators MDH1, MPP7, YAP1, and ULK1 are depleted (Supplementary Figure 3C, 3D).

Discussion

Increasing evidence that PDAC cells require autophagy for survival is supported by studies where pharmacological or genetic inhibition of autophagy caused xenograft regression and cell death (4). However, the mechanisms through which autophagy in PDAC is regulated remain to be determined.

As autophagy is a vital process for cellular homeostasis and plays an important role in malignancies including PDAC, it is of both basic scientific and translational interest to decipher additional autophagy regulators. Previously, high-throughput screening has proven to be a fundamental tool enabling key regulatory protein identification (36, 37). These screens have been performed using overexpressed markers, such as GFP-LC3, which might result in a bias towards overexpression artifacts.

We identified and validated a number of new autophagy regulators in 4 four PDAC cell lines through unbiased loss-of-function screens with a quantifiable endogenous autophagy read-outs. Our hit-selection strategy involved choosing autophagy regulators which that were required for autophagy-dependent PDAC cell survival, and not autophagy-independent PDAC cell survival. This approach revealed a new roles for MDH1 and MPP7. Extensive verification of MPP7 and MDH1 as autophagy regulators used a range of experimental approaches and established that MDH1 and MPP7 impact on autophagy under both basal and hypoxic conditions. It is important to note that while the current study has been performed in PDAC cell lines and organoids, we have not tested the effect of MDH1, MPP7 and downstream proteins in other cancer cell types, or in healthy cells, so we cannot rule out that these proteins regulate autophagy in other contexts.

We propose that MDH1 functions to maintain cellular ULK1 levels, the key autophagy initiator by activation of the class III PI3K and by mediating ATG9 trafficking (38, 39). Our results further suggest that MDH1 prevents proteasomal degradation of ULK1, which has previously been shown to be a mechanism of controlling autophagy (40, 41).

MDH1 is overexpressed in several cancers (41) and contributes to PDAC cell proliferation and metabolism via NAD production to support glycolysis (23, 24). We present a new role for MDH1 in PDAC, where MDH1 contributes to PDAC survival by promoting autophagy. Furthermore, the catalytic activity of MDH1 maybe linked with its ability to indirectly activate autophagy (Supplementary Figure 3E). In addition to its direct effect via ULK1, and MDH1 becomes activated upon autophagic stimuli such as starvation and hypoxia (Supplementary Figure 3F).

Our study reveals MPP7 as a novel positive regulator of PDAC cell survival and autophagy, both in immortalised human pancreatic cancer cells and primary PDAC organoids. A mechanism through which MPP7 regulates autophagy involves YAP1, a transcriptional activator with an established function in PDAC. YAP1 levels are elevated in pancreatic cancer compared to normal pancreas (42), and YAP1 promotes pancreatic cancer in mice via activation of JAK-STAT3 signalling (43). We propose MPP7 promotes YAP1 activation in PDAC cells, which is supported by data in skeletal muscle stem cells (26). Further support of our hypothesis that YAP1 is required, is that two members of the HIPPO pathway, MOBKL1A (ranked 136) and TEAD3 (ranked 67), are in the top 200 autophagy regulators (see Supplementary Table S2). Other data to support of a role for the HIPPO pathway is identification of LC3 as a substrate for the HIPPO kinases MST1/MST2 (44). The role of YAP1 in autophagy requires further investigation, in particular how MPP7 regulates YAP1, and whether YAP1 activates autophagy via its transcriptional activator role or an unidentified cytoplasmic function.

In conclusion, our study highlights MPP7 and MDH1 as key autophagy regulators in PDAC. In hypoxia, both MDH1 and MPP7 are required for autophagy, and MDH1 becomes activated in response to hypoxia. This is of particular translational relevance as poor vasculature and the resulting hypoxic microenvironment are seen in human PDAC (27). Given the importance of autophagy in PDAC cell survival and PDAC progression, this

information provides a significant step forward in developing approaches to exploit the sensitivity of PDAC malignancy to autophagy inhibition.

Supplementary Material

Refer to Web version on PubMed Central for supplementary material.

Acknowledgements

We thank Scott Vande Pol (Department of Pathology, University of Virginia) for pcDNA3-flag-MPP7, Eric Sahai and Anna Dowbaj (Tumour Cell Biology Laboratory, Francis Crick Institute) for EYFP-YAP1-WT and EYFP-S94A and advice, H. D. Youn (Cancer Research Institute, Seoul National University) for pcDNA 3.1-MDH1-Myc, Louise Fets and Dimitrios Anastasiou for advice on MDH1 enzyme activity assay, Thomas Mercer and Alex van Vliet for advice and reading the manuscript.

We acknowledge the support of Astellas Pharma, and in particular Kyouko Saita, Hiromichi Kimura and Takatoshi Soga for scientific discussions. We also thank Chris Baker (Cancer Research Technology) for project management and scientific discussions.

Funding

The work in the Tooze lab (ST, MN, TVA) and the High Throughput Screening Facility (MH, BS, MJ) was supported by the Francis Crick Institute which receives its core funding from Cancer Research UK (FC001187, FC001999), the UK Medical Research Council (FC001187, FC001999), and the Wellcome Trust (FC001187, FC001999). The work in the Ryan lab (KR) was funded by Cancer Research UK (C596/A17196). MN, TVA, JS, JL were funded by Astellas Pharma as part of a sponsored research collaboration. The work in the Behrens lab (AB and VMYW) was supported by the Francis Crick Institute which receives its core funding from Cancer Research UK (FC001039), the UK Medical Research Council (FC001039), and the Wellcome Trust (FC001039). TK was supported by a fellowship in computational biology at Earlham Institute (Norwich, UK) in partnership with the Quadram Institute (Norwich, UK), and strategically supported by Biotechnological and Biosciences Research Council, UK (BB/J004529/1 and BB/P016774/1).

References

1. Siegel RL, Miller KD, Jemal A. Cancer Statistics, 2017. *CA Cancer J Clin.* 2017; 67(1):7–30. [PubMed: 28055103]
2. Ryan DP, Hong TS, Bardeesy N. Pancreatic Adenocarcinoma. *New England Journal of Medicine.* 2014; 371(11):1039–1049. [PubMed: 25207767]
3. Yang S, et al. Pancreatic cancers require autophagy for tumor growth. *Genes & Development.* 2011; 25(7):717–729. [PubMed: 21406549]
4. Yang A, et al. Autophagy Sustains Pancreatic Cancer Growth through Both Cell-Autonomous and Nonautonomous Mechanisms. *Cancer Discovery.* 2018; 8(3):276–287. [PubMed: 29317452]
5. Lamb CA, Yoshimori T, Tooze SA. The autophagosome: origins unknown, biogenesis complex. *Nat Rev Mol Cell Biol.* 2013; 14(12):759–774. [PubMed: 24201109]
6. Slobodkin MR, Elazar Z. The Atg8 family: multifunctional ubiquitin-like key regulators of autophagy. *Essays Biochem.* 2013; 55:51–64. [PubMed: 24070471]
7. Yoshii SR, Mizushima N. Monitoring and Measuring Autophagy. *International Journal of Molecular Sciences.* 2017; 18(9):1865.
8. Galluzzi L, et al. Autophagy in malignant transformation and cancer progression. 2015:856–880.
9. Perera RM, et al. Transcriptional control of autophagy-lysosome function drives pancreatic cancer metabolism. *Nature.* 2015; 524:361–365. [PubMed: 26168401]
10. Yang A, et al. Autophagy is critical for pancreatic tumor growth and progression in tumors with p53 alterations. *Cancer Discovery.* 2014
11. Joachim J, et al. Activation of ULK Kinase and Autophagy by GABARAP Trafficking from the Centrosome Is Regulated by WAC and GM130. *Molecular Cell.* 2015; 60(6):899–913. [PubMed: 26687599]

12. Dooley HC, et al. WIPI2 links LC3 conjugation with PI3P, autophagosome formation, and pathogen clearance by recruiting Atg12-5-16L1. *Mol Cell*. 2014; 55(2):238–252. [PubMed: 24954904]
13. Turei D, et al. Autophagy Regulatory Network - a systems-level bioinformatics resource for studying the mechanism and regulation of autophagy. *Autophagy*. 2015; 11(1):155–165. [PubMed: 25635527]
14. Orchard S, et al. The MIntAct project--IntAct as a common curation platform for 11 molecular interaction databases. *Nucleic Acids Res*. 2014; 42(Database issue):D358–363. [PubMed: 24234451]
15. Keshava Prasad TS, et al. Human Protein Reference Database--2009 update. *Nucleic Acids Res*. 2009; 37(Database issue):D767–772. [PubMed: 18988627]
16. Bovolenta LA, Acencio ML, Lemke N. HTRIdb: an open-access database for experimentally verified human transcriptional regulation interactions. *BMC Genomics*. 2012; 13:405. [PubMed: 22900683]
17. Lesurf R, et al. ORegAnno 3.0: a community-driven resource for curated regulatory annotation. *Nucleic Acids Res*. 2016; 44(D1):D126–132. [PubMed: 26578589]
18. Uhlen M, et al. Proteomics. Tissue-based map of the human proteome. *Science*. 2015; 347(6220)
19. Nagpal G, et al. PCMDB: pancreatic cancer methylation database. *Sci Rep*. 2014; 4
20. Bardeesy N, et al. Both p16^{Ink4a} and the p19^{Arf}-p53 pathway constrain progression of pancreatic adenocarcinoma in the mouse. *Proceedings of the National Academy of Sciences*. 2006; 103(15): 5947–5952.
21. Boj Sylvia F, et al. Organoid Models of Human and Mouse Ductal Pancreatic Cancer. *Cell*. 2015; 160(1):324–338. [PubMed: 25557080]
22. Son J, et al. Glutamine supports pancreatic cancer growth through a KRAS-regulated metabolic pathway. *Nature*. 2013; 496(7443):101–105. [PubMed: 23535601]
23. Hanse EA, et al. Cytosolic malate dehydrogenase activity helps support glycolysis in actively proliferating cells and cancer. *Oncogene*. 2017; 36(27):3915–3924. [PubMed: 28263970]
24. Wang YP, et al. Arginine Methylation of MDH1 by CARM1 Inhibits Glutamine Metabolism and Suppresses Pancreatic Cancer. *Mol Cell*. 2016; 64(4):673–687. [PubMed: 27840030]
25. Bohl J, Brimer N, Lyons C, Vande Pol SB. The stardust family protein MPP7 forms a tripartite complex with LIN7 and DLG1 that regulates the stability and localization of DLG1 to cell junctions. *J Biol Chem*. 2007; 282(13):9392–9400. [PubMed: 17237226]
26. Li L, Fan CM. A CREB-MPP7-AMOT Regulatory Axis Controls Muscle Stem Cell Expansion and Self-Renewal Competence. *Cell Rep*. 2017; 21(5):1253–1266. [PubMed: 29091764]
27. Koong AC, et al. Pancreatic tumors show high levels of hypoxia. *Int J Radiat Oncol Biol Phys*. 2000; 48(4):919–922. [PubMed: 11072146]
28. Chang Q, Jurisica I, Do T, Hedley DW. Hypoxia predicts aggressive growth and spontaneous metastasis formation from orthotopically grown primary xenografts of human pancreatic cancer. *Cancer Res*. 2011; 71(8):3110–3120. [PubMed: 21343390]
29. Bellot G, et al. Hypoxia-induced autophagy is mediated through hypoxia-inducible factor induction of BNIP3 and BNIP3L via their BH3 domains. *Molecular and cellular biology*. 2009; 29(10): 2570–2581. [PubMed: 19273585]
30. McAlpine F, Williamson L, Tooze SA, Chan EYW. Regulation of nutrient-sensitive autophagy by uncoordinated-51 like kinases 1 and 2. *Autophagy*. 2013; 9:361–373. [PubMed: 23291478]
31. Joachim J, et al. Activation of ULK kinase and autophagy by GABARAP trafficking from the centrosome is regulated by WAC and GM130. *Molecular Cell*. 2015; 60:899–913. [PubMed: 26687599]
32. Song Q, et al. YAP enhances autophagic flux to promote breast cancer cell survival in response to nutrient deprivation. *PLoS One*. 2015; 10(3):e0120790. [PubMed: 25811979]
33. Oldham WM, Clish CB, Yang Y, Loscalzo J. Hypoxia-Mediated Increases in L-2-hydroxyglutarate Coordinate the Metabolic Response to Reductive Stress. *Cell Metab*. 2015; 22(2):291–303. [PubMed: 26212716]

34. Breiter DR, Resnik E, Banaszak LJ. Engineering the quaternary structure of an enzyme: construction and analysis of a monomeric form of malate dehydrogenase from *Escherichia coli*. *Protein Sci.* 1994; 3(11):2023–2032. [PubMed: 7703849]
35. Campbell M, et al. Protein arginine methyltransferase 1-directed methylation of Kaposi sarcoma-associated herpesvirus latency-associated nuclear antigen. *J Biol Chem.* 2012; 287(8):5806–5818. [PubMed: 22179613]
36. Lipinski MM, et al. Genome-wide analysis reveals mechanisms modulating autophagy in normal brain aging and in Alzheimer's disease. *Proc Natl Acad Sci U S A.* 2010; 107(32):14164–14169. [PubMed: 20660724]
37. McKnight NC, et al. Genome-wide siRNA screen reveals amino acid starvation-induced autophagy requires SCOC and WAC. *EMBO J.* 2012; 31(8):1931–1946. [PubMed: 22354037]
38. Russell RC, et al. ULK1 induces autophagy by phosphorylating Beclin-1 and activating VPS34 lipid kinase. *Nat Cell Biol.* 2013
39. Young ARJ, et al. Starvation and ULK1-dependent cycling of Mammalian Atg9 between the TGN and endosomes. *J Cell Sci.* 2006; 119:3888–3900. [PubMed: 16940348]
40. Nazio F, et al. mTOR inhibits autophagy by controlling ULK1 ubiquitylation, self-association and function through AMBRA1 and TRAF6. *Nat Cell Biol.* 2013; 15(4):406–416. [PubMed: 23524951]
41. Allavena G, et al. Suppressed translation and ULK1 degradation as potential mechanisms of autophagy limitation under prolonged starvation. *Autophagy.* 2016; 12(11):2085–2097. [PubMed: 27629431]
42. Morvaridi S, Dhall D, Greene MI, Pandol SJ, Wang Q. Role of YAP and TAZ in pancreatic ductal adenocarcinoma and in stellate cells associated with cancer and chronic pancreatitis. *Sci Rep.* 2015; 5:16759. [PubMed: 26567630]
43. Gruber R, et al. YAP1 and TAZ Control Pancreatic Cancer Initiation in Mice by Direct Up-regulation of JAK-STAT3 Signaling. *Gastroenterology.* 2016; 151(3):526–539. [PubMed: 27215660]
44. Wilkinson DS, et al. Phosphorylation of LC3 by the Hippo kinases STK3/STK4 is essential for autophagy. *Mol Cell.* 2015; 57(1):55–68. [PubMed: 25544559]

Statement of significance

This study identifies and characterises MPP7 and MDH1 as novel regulators of autophagy, which is thought to be responsible for pancreatic cancer cell survival.

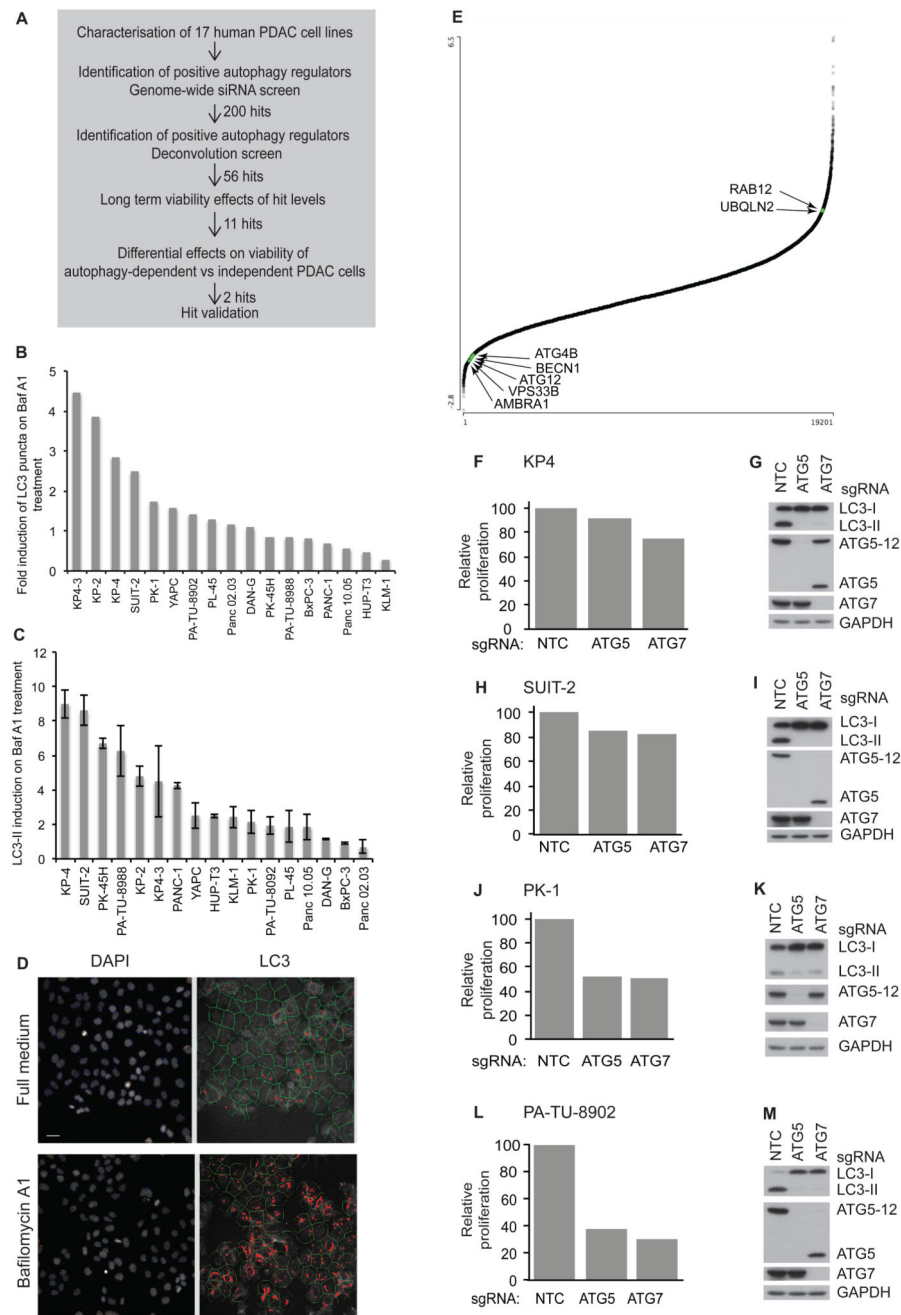


Figure 1. siGENOME screen reveals novel autophagy regulators in PDAC cells.

A) Screen summary indicating the autophagy regulator (“hit”) selection procedure. **B)** PDAC cell lines were treated with Bafilomycin A1 (BafA1) for 2 hour, fixed, labelled with LC3, and LC3 puncta quantified (Mean of n=2), or **C)** analysed by immunoblot, and quantified. LC3II (BafA1)/LC3II (Full media), mean ± SD, n=2. **D)** Images from siGENOME screen of RISC-free (RF) siRNA transfected, BafA1 treated cells. In the bottom panels, cell outlines are indicated in green, LC3 puncta in red. Scale bar 20 µm. **E)** Scatter plot of median spot total area per object (STAPO) Z-scores from siRNA pools in the primary screen plotted

against rank. Examples of known autophagy genes are indicated with arrows. **F - M** PDAC cell lines were infected with non-targeting control (NTC), ATG5 or ATG7 sgRNAs. 7 days after infection cell were counted, and ATG5 and ATG7 depletion confirmed by immunoblot analysis, n=2 for all cell lines

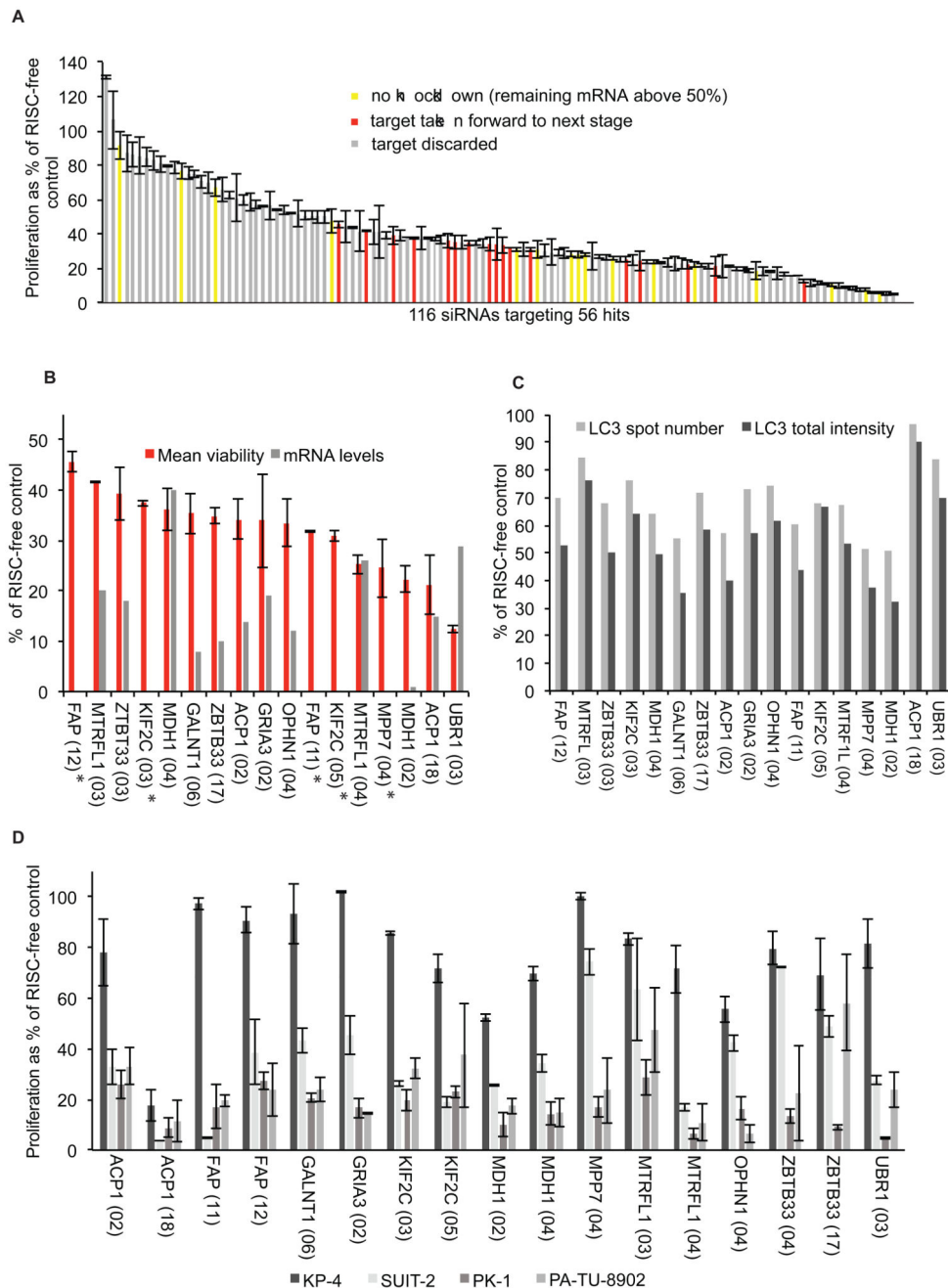


Figure 2. MDH1 and MPP7, novel autophagy regulators are needed for survival of autophagy-dependent PDAC cell lines.

A) A high-throughput 96-well format colony formation assay (CFA) in PK-1 cells. 7 days after deconvoluted siRNAs were reverse transfected, cells were fixed, and Hoechst stained. Cell number/96-well was determined and normalised to RF siRNA transfected cells. Mean and SD, n=2. 11 selected autophagy regulators are highlighted in red, siRNAs with a knockdown efficiency below 50% by qPCR are in yellow. **B**) Cell viability and knockdown efficiency for the CFA in A for the 11 hits taken forward. (*) indicates qPCR data was

inconclusive. **C)** siRNA depletion of the top 25% siGENOME KP-4 screen hits was assessed in the PK-1 cell line (n=1). Reverse siRNA transfection in a 384-well format as done in the siGENOME KP-4 screen. Total LC3 intensity and spot number shown for the 11 hits taken to the next stage of analysis. **D)** A high-throughput long-term growth assay was performed in the autophagy-dependent PK-1 and PA-TU-8902 and autophagy-independent KP-4 and SUIT-2 cell lines. Reverse siRNA transfected cells (4 96-wells/condition), grown for 7 days, were fixed and stained with Hoechst. Cell number/96-well was normalised to RF siRNA transfected cells. siRNAs which were on-target (previously shown by qPCR) were used in this assay. Mean and SD, n=2.

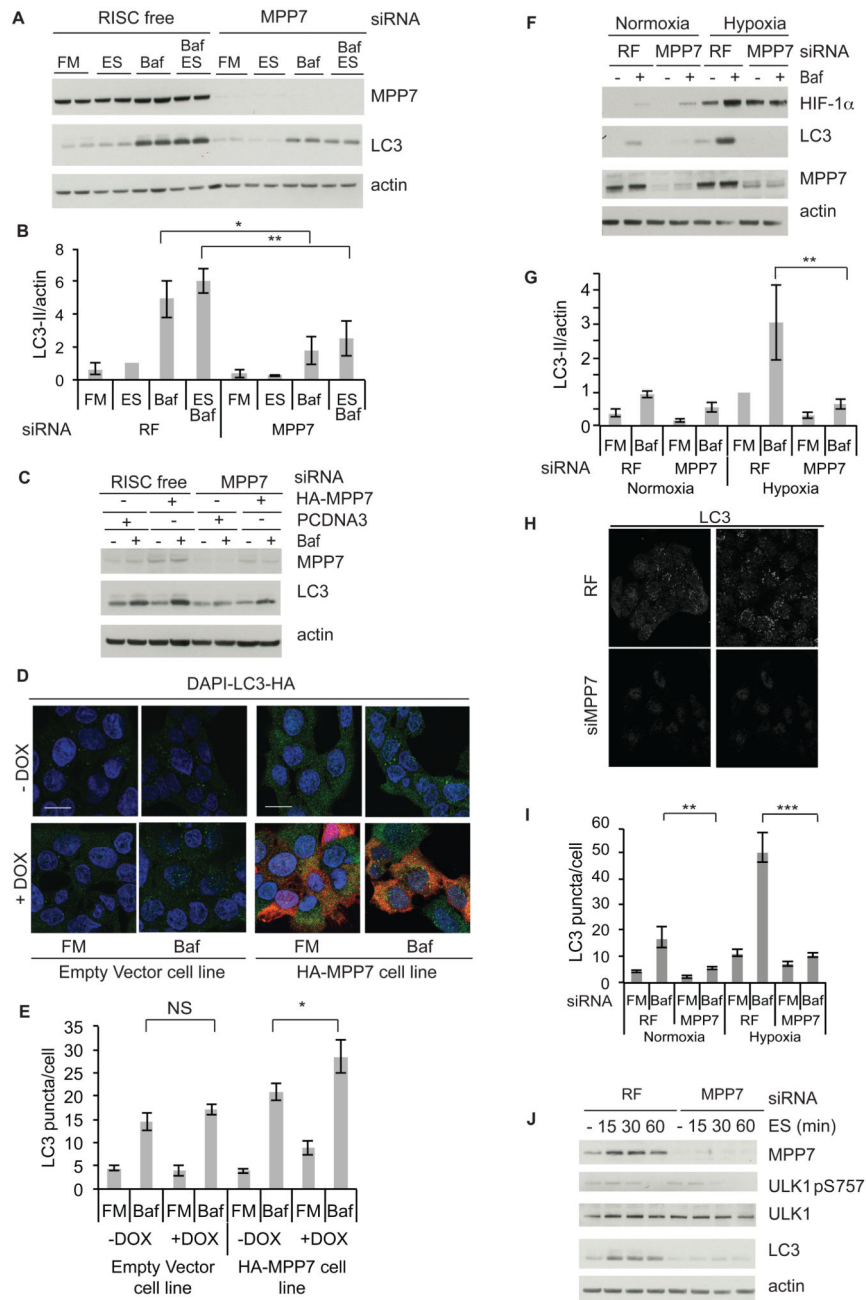


Figure 3. MPP7 regulates basal and hypoxia induced autophagy.

A) PK-1 cells treated for 72 hours with RF or MPP7 siRNA, starved for 4 hours with EBSS (ES) or BafA1 (Baf) and analysed. **B)** Quantification of A, mean \pm SD, $n = 3$, * $p < 0.05$, ** $p < 0.01$, unpaired Student's t test. **C)** PK-1 cells treated for 72 hours RF or MPP7 siRNA, were transfected with siRNA-resistant HA-MPP7 or empty vector for final 24 hours. Cells were treated with or without BafA1 for 4 hours and analysed. **D)** PK-1 cells stably expressing Tet-On HA-tagged MPP7 noninduced (-) or induced (+) with doxycycline (DOX) were treated with BafA1 for 2 hours. Cells were fixed, and labelled with the

indicated antibodies. Scale bar 20 μm . **E)** Quantification of D, mean \pm SEM, unpaired Student's t test. **F)** PK-1 cells, treated for 72 hours with RF or MPP7 siRNA were incubated in 0.1% oxygen for 24 hour and treated with BafA1 for final 4 hours and analysed. **G)** Quantification of F. Mean \pm SD, n = 3, ** p < 0.01, unpaired Student's t test. **H)** PK-1 cells were treated as in F, were fixed, and labelled with the indicated antibodies. Only BafA1 treated cells are presented. Scale bar 20 μm . **I)** Quantification of LC3 puncta in H, mean \pm SEM, unpaired Student's t test. **J)** PK-1 cells were treated for 72 hours with RF or MPP7 siRNA, and starved (ES) for the indicated times then analysed by immunoblotting, n=3.

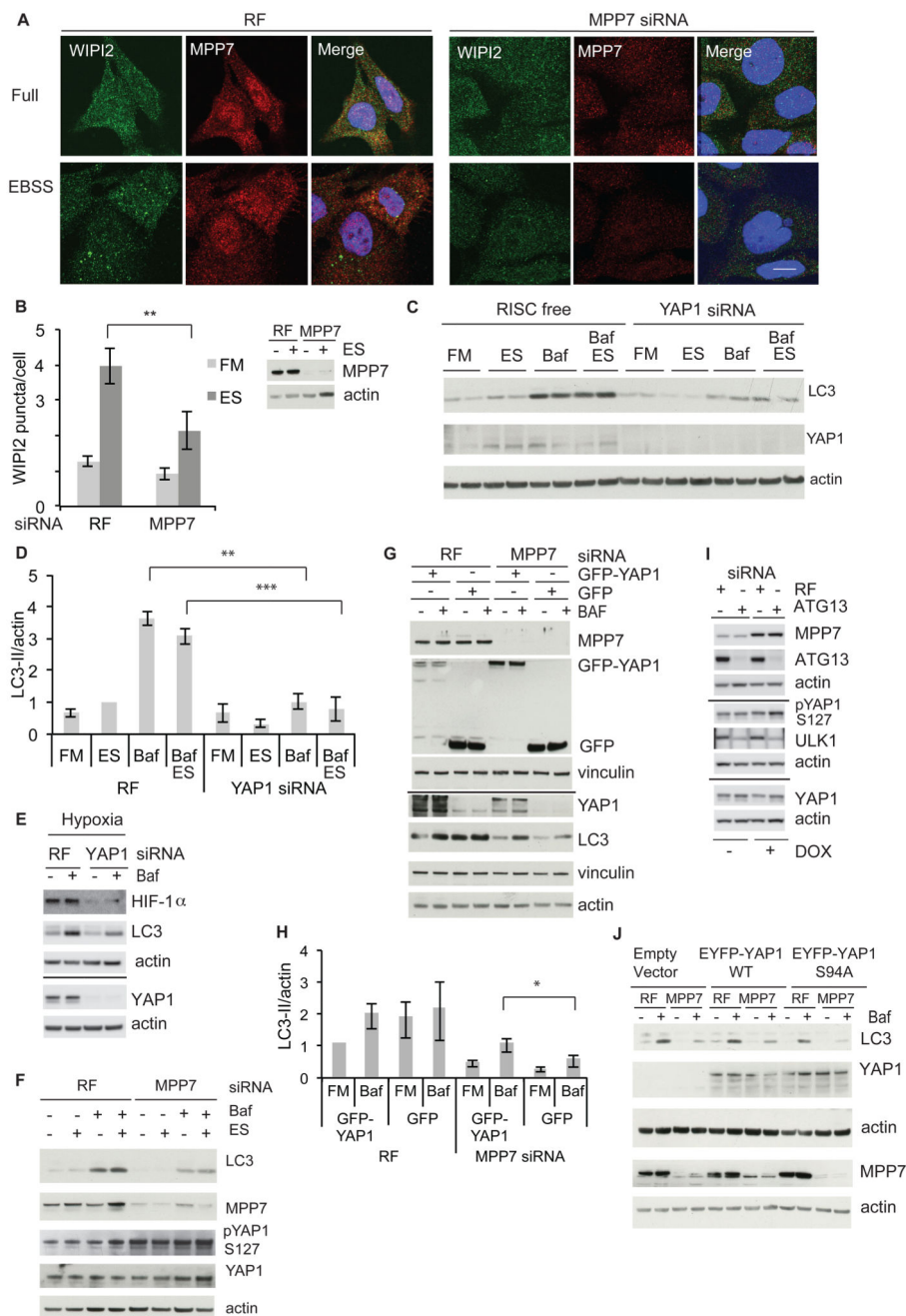


Figure 4. MPP7 regulates autophagy through YAP1 activation.

A) PK-1 cells were treated for 72 hours with RF or MPP7 siRNA, and starved in EBSS for 2 hours, followed by labelling with the indicated antibodies. Scale bar 20 μ m. **B)** Quantification of intracellular WIPI2 puncta in A. Mean \pm SEM, unpaired Student's t test. **C)** PK-1 cells were treated for 72 hours with RF or YAP1 siRNA, and starved without or with BafA1 for 4 hour, then analysed. **D)** Quantification of C. Mean \pm SD, n = 3, ** p 0.01, *** p 0.001, unpaired Student's t test. **E)** PK-1 cells treated for 72 hours with RF or YAP1 siRNA, were incubated in 0.1% oxygen for 24 hours, without or with BafA1 for final

4 hours and analysed. **F)** PK-1 cells were treated for 72 hours with RF or MPP7 siRNA, starved, and/or treated with BafA1 for 4 hours, then analysed, n=3. **G)** PK-1 cells were treated for 72 hours with RF or MPP7 siRNA, and transfected with GFP-YAP1 or empty vector for final 24 hours. Cells were treated with BafA1 for 4 hour and analysed, two blots were performed (separated by a line), with loading controls for each. **H)** Quantification of G. Mean \pm SD, n = 3, * p < 0.05, unpaired Student's t test. **I)** PK-1 cells stably expressing Tet-On HA-tagged MPP7 were without (-) or with (+) DOX for 72 hours, treated with RF siRNA or Atg13 siRNA for 72 hours, and analysed. Three blots were performed, separated by lines. **J)** PK-1 cells stably expressing EYFP-YAP1 WT, EYFP-YAP1 S94A or empty vector were treated for 72 hours with RF or MPP7 siRNA, then without or with BafA1 for 4 hours, analysed. Two blots were performed, separated by a line.

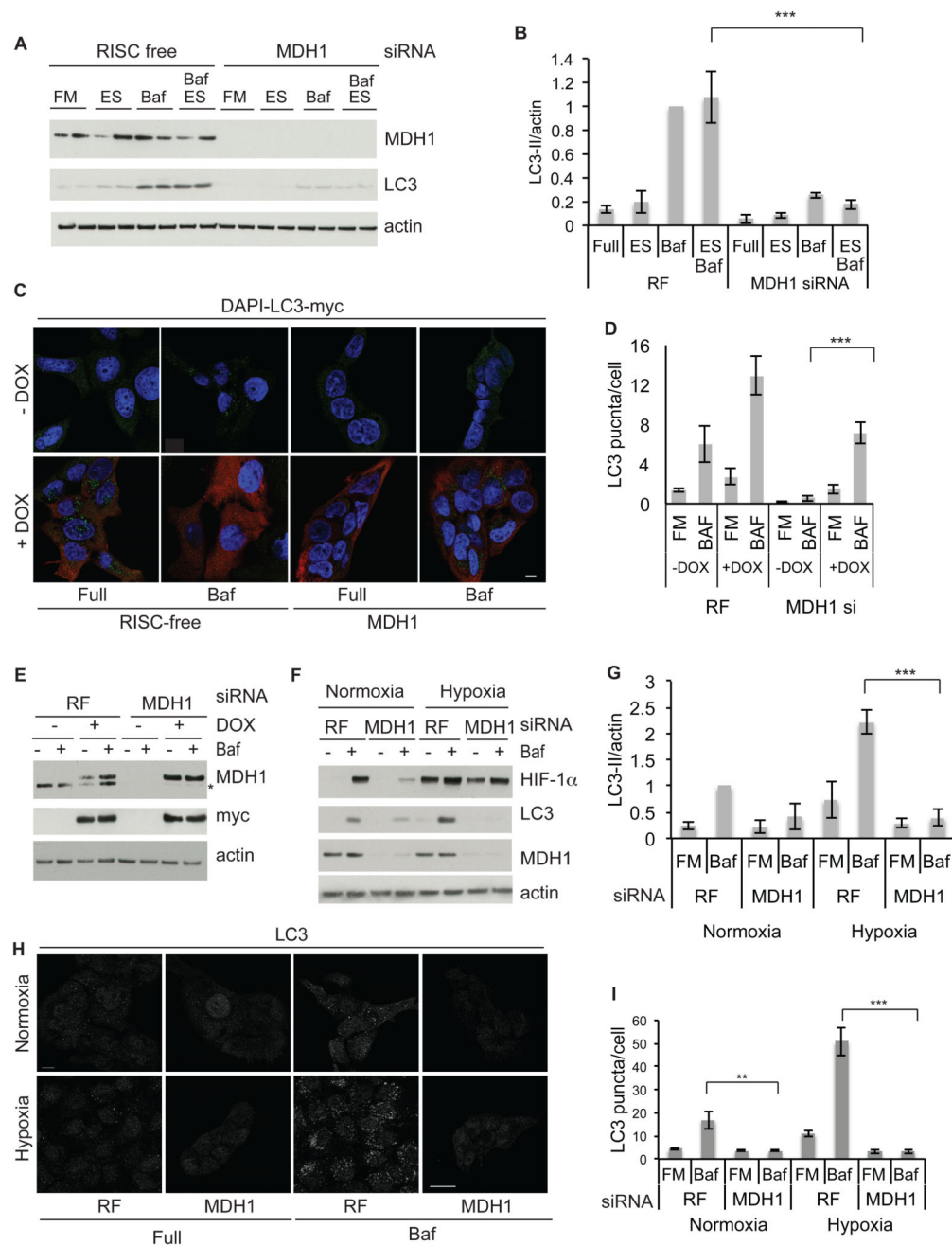


Figure 5. MDH1 regulates basal and hypoxia induced autophagy.

A) PK-1 cells were treated for 72 hours with RF or MDH1 siRNA. After 4 hours starvation (ES) with or without BafA1, cells were analysed. **B)** Quantification of A. Mean \pm SD, $n = 3$, *** $p < 0.001$, unpaired Student's t test. **C)** PK-1 cells stably expressing Tet-On myc-tagged siRNA resistant MDH1 were grown without (-) or with (+) DOX, incubated for 72 hours with RF or MDH1 siRNA, then with or without BafA1 for 4 hour, fixed and labelled with anti-myc. Scale bar 20 μ m. **D)** Quantification of intracellular puncta in C. Mean \pm SEM, unpaired Student's t test. **E)** Cells treated as in C analysed by immunoblot. Endogenous

MDH1 indicated by *. **F)** PK-1 cells were treated for 72 hours with RF or MDH1 siRNA, incubated in 0.1% oxygen for 24 hours. Cells were treated with BafA1 for 4 hours and analysed. **G)** Quantification of F. Mean \pm SD, n = 3, ** p < 0.01, unpaired Student's t test. **H)** PK-1 cells were treated for 72 hours with RF or MDH1 siRNA, incubated in at 0.1% oxygen for 24 hours. Cells were treated with BafA1 for 4 hours, fixed, and labelled with anti-LC3. Scale bar 20 μ m. **I)** Quantification of LC3 puncta in H. Mean \pm SEM, unpaired Student's t test.

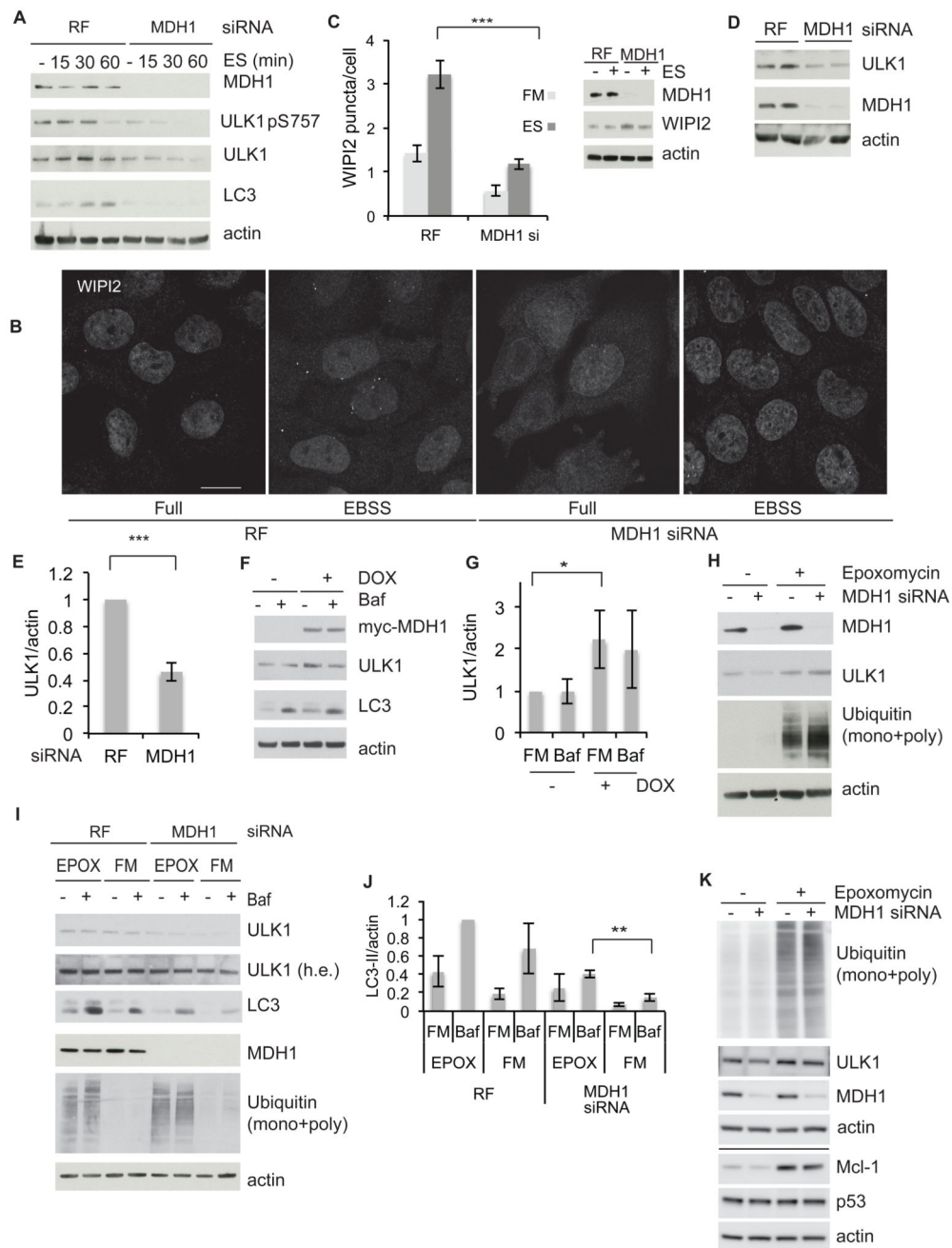


Figure 6. MDH1 regulates autophagy by maintaining ULK1 levels.

A) PK-1 cells were treated for 72 hours with RF or MDH1 siRNA, starved in EBSS and analysed. **B)** PK-1 cells were treated for 72 hours with RF or MDH1 siRNA, and starved for 2 hours, followed by labelling with anti-WIPI2. Scale bar 20 μ m. **C)** Quantification of WIPI2 puncta in B. Mean \pm SEM, unpaired Student's t test. Immunoblot confirms knockdown in B and C. **D)** PK-1 cells were treated for 72 hours with RF or MDH1 siRNA, then analysed. **E)** Quantification of D. Mean \pm SD, n = 3; *** p < 0.001, unpaired Student's t test. **F)** PK-1 cells stably expressing Tet-On myc-tagged MDH1 grown without (-) or with

(+) DOX for 72 hours, treated with RF siRNA for 72 hours, and then without or with BafA1 for the final 4 hours, and analysed. **G)** Quantification of F. Mean \pm SD, n = 3; ** p < 0.01, unpaired Student's t test. **H)** PK-1 cells were treated for 72 hours with RF or MDH1 siRNA and epoxomycin (100nM) for 8 hours, then analysed by immunoblotting, n=3. **I)** PK-1 cells were treated for 72 hours with RF or MDH1 siRNA and epoxymycin for 8 hours, and BafA1 for the final 4 hours, then analysed. **J)** Quantification of I. Mean \pm SD, n = 3, ** p < 0.01, unpaired Student's t test. **K)** PK-1 cells were treated for 72 hours with RF or MDH1 siRNA and epoxomycin for 8 hours, then analysed, n=3.

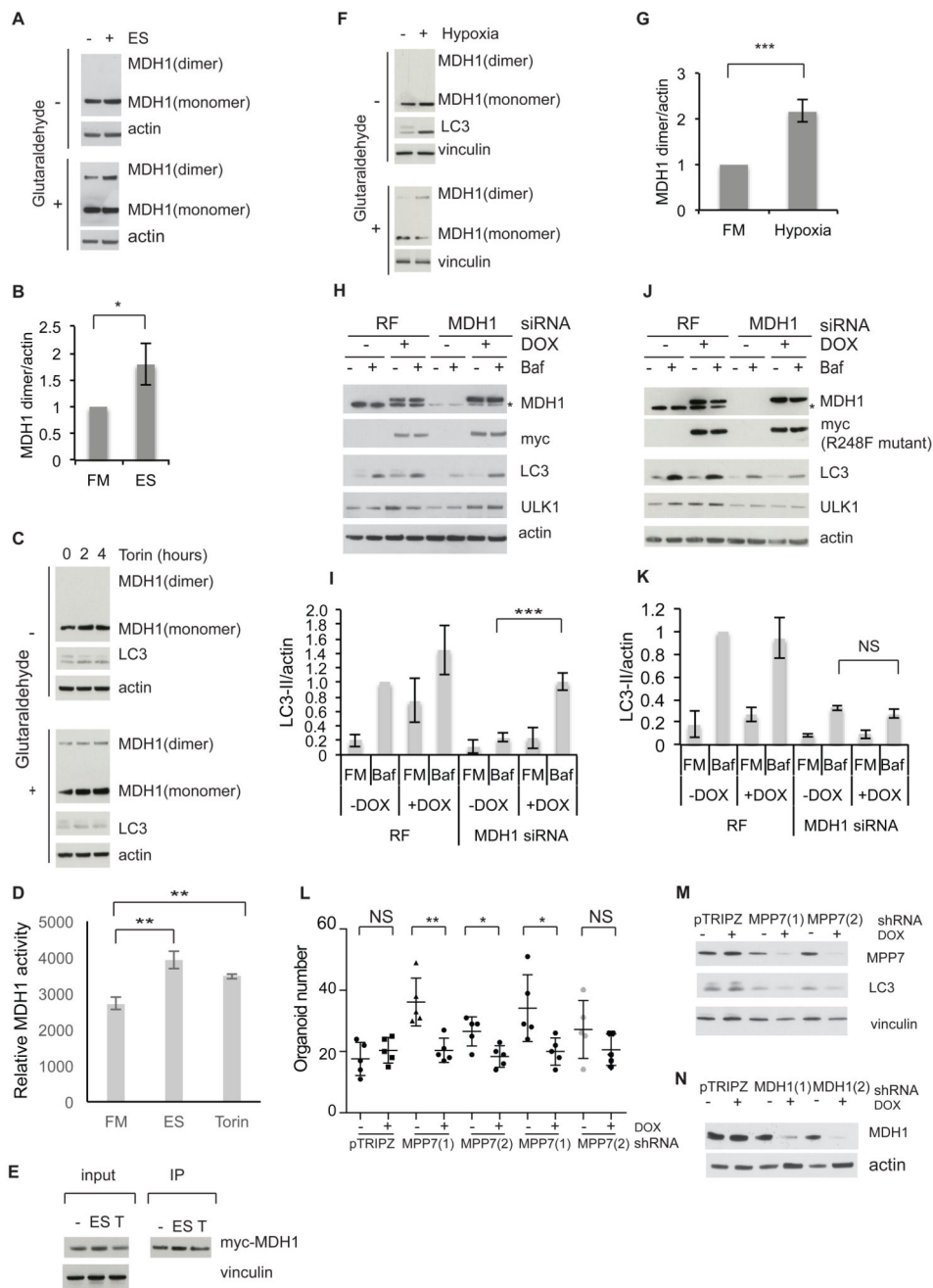


Figure 7. MDH1 is activated by autophagic stimuli

A) PK-1 cells were starved for 4 hours. MDH1 dimerization was preserved through 0.05 % glutaraldehyde crosslinking. **B)** Quantification of A. Mean \pm SD, n = 3; * p < 0.05, unpaired Student's t test. **C)** PK-1 cells treated with 100nM Torin followed by 0.05% glutaraldehyde crosslinking. **D)** PK-1 cells stably expressing Tet-On myc-tagged MDH1 were grown with DOX for 72 hours, followed by immunoprecipitation of myc-MDH1. MDH1 activity was then assessed measuring NADH fluorescence, n=3. Mean \pm SD, triplicate wells/condition, ** p < 0.01, *** p < 0.001, unpaired Student's t test. **E)** Immunoprecipitation in D was

analysed by immunoblot. **F)** PK-1 cells were incubated in 0.1% oxygen for 24 hours where indicated followed by 0.05% glutaraldehyde crosslinking. **G)** Quantification of F. Mean \pm SD, n = 3; *** p < 0.001, unpaired Student's t test. **H)** PK-1 cells stably expressing wild type Tet-On myc-tagged MDH1 were grown without (-) or with (+) DOX for 72 hours, treated for 72 hours with RF or MDH1 siRNA, then BafA1 for the final 4 hours, followed by analysis. Endogenous MDH1 indicated by *. **I)** Quantification of H. Mean \pm SD, n = 3; *** p < 0.001, unpaired Student's t test. **J)** PK-1 cells stably expressing Tet-On myc-tagged R230F MDH1 were without (-) or with (+) DOX for 72 hours, treated with 72 hours RF or MDH1 siRNA and treated with BafA1 for the final 4 hours, followed by analysis. Endogenous MDH1 is indicated by *. **K)** Quantification of J. Mean \pm SD, n = 3, unpaired Student's t test. **L)** Mouse PDAC cells expressing doxycycline-inducible pTRIPZ empty vector control, pTRIPZ-MPP7 and pTRIPZ-MDH1 targeting shRNAs were grown in the without (-) or with (+) of DOX for 72 hours. 200 cells/well were FACS-sorted into Matrigel to allow organoid growth in 3D, 5 96-wells/condition. Cells were grown without (-) or with (+)DOX for 6 days. Organoid number/well was measured with ImageJ. Statistical analysis was performed using, ** p < 0.01, unpaired Student's t test, n=2. **M), N)** Cells from (L) analysed to confirm knockdown.